Applied Problems of Nonlinear Oscillation and Wave Theory

Izvestiya Vysshikh Uchebnykh Zavedeniy. Applied Nonlinear Dynamics. 2025;33(6)

Article DOI: 10.18500/0869-6632-003187

Modulation instability and soliton formation under interaction of an electromagnetic wave with a beam of unexcited non-isochronous electron-oscillators

N. S. Ginzburg[1], *V. Yu. Zaslavsky*[1], *I. V. Zotova*[1], *A. A. Rostuntsova*[1,2,3] ✉, *N. M. Ryskin*[2,3], *A. S. Sergeev*[1], *L. A. Yurovskiy*[1]

[1]FRC A. V. Gaponov-Grekhov Institute of Applied Physics of the RAS, Nizhny Novgorod, Russia
[2]Saratov Branch of Kotelnikov Institute of Radioengineering and Electronics of the RAS, Russia
[3]Saratov State University, Russia

E-mail: ginzburg@ipfran.ru, zas-vladislav@ipfran.ru, zotova@appl.sci-nnov.ru, ✉rostuncova@mail.ru, ryskinnm@info.sgu.ru, sergeev@ipfran.ru, leo@ipfran.ru

Received 14.05.2025, accepted 10.06.2025, available online 9.07.2025, published 28.11.2025

Abstract. This paper develops the theory of modulation instability (MI) in the interaction of an electromagnetic wave with a counterpropagating beam of unexcited electron-oscillators under the cyclotron resonance conditions. The *purpose* of this study is to establish the pattern of possible wave propagation regimes in such a system. *Methods.* The theoretical analysis is based on the nonlinear Schrödinger equation, which enables to determine the conditions for occurrence of MI and obtain a simple analytical expression for the boundary between the absolute and convective MI on the wave frequency — wave amplitude parameter plane. The theoretical conclusions about possible regimes of wave propagation are verified by direct 3D particle-in-cell (PIC) simulation of the electron-wave interaction. The obtained *results* show that above the boundary of cyclotron absorption band non-stationary self-modulation regimes occur. These regimes are caused by absolute MI and can lead to the formation of soliton-like pulse trains. As the frequency of the input signal increases, self-modulation is replaced by a stationary single-frequency regime of wave propagation. This transition is due to the change of MI character from absolute to convective. The results of 3D PIC simulation are consistent with the theoretical analysis of the averaged equations, and the same sequence of transitions between different dynamic regimes occurs as the input frequency increases. *Conclusion.* 3D PIC simulation provided an opportunity to study a model that approximates the conditions of a potential experiment. The possibility of converting the 241.3-GHz signal into a close-to-periodic train of nanosecond pulses was demonstrated. Such an effect is useful for the generation of microwave frequency combs.

Keywords: modulation instability, self-induced transparency, microwave solitons, cyclotron resonance.

Acknowledgements. This work was supported by Russian Science Foundation under Grant No. 23-12-00291.

For citation: Ginzburg NS, Zaslavsky VYu, Zotova IV, Rostuntsova AA, Ryskin NM, Sergeev AS, Yurovskiy LA. Modulation instability and soliton formation under interaction of an electromagnetic wave with a beam of unexcited non-isochronous electron-oscillators. Izvestiya VUZ. Applied Nonlinear Dynamics. 2025;33(6):823–842. DOI: 10.18500/0869-6632-003187

Introduction

In nonlinear physics, an approach based on analogies between phenomena observed in systems of different physical nature has proven to be quite fruitful. In particular, it is well known that many effects in systems of the «electron beam is electromagnetic field» type have analogs in nonlinear optics [1,2]. One such effect is self-induced transparency (SIT), which arises when a short light pulse with a duration much shorter than the relaxation times propagates in a two-level passive (non-inverted) medium [3]. Under resonance conditions, when the wave frequency is close to the transition frequency, unexcited particles, absorbing the field energy, make a transition to an excited level and weaken the leading edge of the pulse. Under such conditions, the trailing edge of the pulse propagates in an already excited medium, causing reverse transitions of the particles, accompanied by an amplification of the corresponding sections of the pulse profile. As a result, the pulse acquires an equilibrium soliton-like shape and propagates at a constant velocity as a stationary solitary wave [4]. Moreover, a pulse with sufficiently high energy can decay into several SIT solitons.

As shown in [5–8], in classical microwave electronics, a phenomenon analogous to SIT occurs during the resonant interaction of an electromagnetic wave (EMW) with a beam of unexcited cyclotron electron oscillators. In a beam of electrons moving in a longitudinal magnetic field, the transverse motion of the electrons is rotation with a cyclotron frequency ω_H. Such an electron beam can be interpreted as a set of cyclotron oscillators, which are non-isochronous due to the relativistic dependence of the cyclotron frequency on energy [9]. If the beam is initially rectilinear, that is, there is no rotational velocity, then such a medium is unexcited.

It's important to note that in vacuum microwave electronics, unlike quantum optics, relaxation processes such as electron-electron collisions or collisions with the ion background are generally insignificant. Thus, new regimes arise that are impossible to observe in laser systems. In particular, numerical simulation results show that, when electrons and waves propagate in opposite directions, a continuous signal of constant amplitude can be transformed into a nearly periodic train of microwave solitons [6–8]. This effect is of obvious interest from the point of view of periodic generation of short pulses with a spectrum in the form of a frequency comb, which is relevant for a number of practical applications, in particular, in spectroscopy [10,11]. Also, in [6–8], numerical simulations demonstrated the generation of more complex, chaotic trains of short pulses was obtained.

In our previous studies [12,13], we showed that the generation of solitons in this system is associated with the development of modulation instability (MI), which is the instability of a monochromatic wave with a carrier frequency ω relative to slow modulations at the side frequencies $\omega \pm \Omega$, $\Omega \ll \omega$. MI is observed in systems of various nature, including optical fibers, electromagnetic transmission lines, waves on the water surface, various types of waves in plasma, etc. [14–16]. As the results of theoretical analysis and numerical simulation have shown, the situation significantly depends on whether the MI is absolute or convective [13]. During convective instability, growing modulation perturbations shift along the system and leave it, resulting in the establishment of a steady-state, single-frequency signal propagation regime at the end of the transient process. However, if the instability is absolute, these perturbations fill the entire interaction space, resulting in the input signal being transformed into a train of traveling solitons [12,13]. Note that in quantum optics, unlike in the situation under consideration, it is impossible to observe the MI of a continuous signal, since relaxation processes inevitably suppress such instability.

This article presents the theory of MI and the formation of microwave SIT solitons in the system «backward electromagnetic wave is beam of unperturbed non-isochronous electron oscillators». The analysis previously conducted using the averaged equations [12,13] is supplemented by direct 3D simulation of the electron-wave interaction using the particle-in-cell (PIC) method in the CST Studio Suite software package [17]. This allows not only to verify the physical picture obtained using the simplified approach but also to explore in more detail a situation close to the conditions of a possible experiment, including determining the main quantitative characteristics of the generated microwave soliton trains.

1. Model and basic equations

The model under study is shown in Fig. 1. Annular electron beam, guided by an axial magnetic field B_0, interacts with a backward EMW in a cylindrical waveguide. Electrons are injected through the

left boundary of the system (at the point $z = 0$) with a constant axial velocity V_z and zero rotational velocity. Thus, the electron beam is initially rectilinear. A continuous harmonic signal with constant amplitude is applied at the right boundary of the system ($z = l$).

Effective interaction of electrons and EMW occurs under conditions of cyclotron resonance, that is, under the condition of synchronism of the waveguide TE_{mn}-mode and the fast cyclotron wave in the electron beam:

$$\omega_r \approx k_z V_z + \omega_H, \tag{1}$$

where $\omega_r = \omega_r(k_z)$ is the wave frequency, k_z is the longitudinal wave number (in the case when the wave is backward, $k_z < 0$), $\omega_H = eB_0/(m_e\gamma)$ is the cyclotron frequency, $\gamma = (1 - V_z^2/c^2)^{-1/2}$, e and m_e are the charge and rest mass of an electron, respectively.

An electron beam moving in a uniform magnetic field can be treated as an ensemble of oscillators that are non-isochronous due to the relativistic dependence of the cyclotron frequency on energy $\omega_H = \omega_H(\gamma)$ [9]. An initially rectilinear electron beam can be considered a passive medium of unperturbed cyclotron oscillators. When an electromagnetic wave propagates toward such an electron beam under resonance conditions (1), it begins to be absorbed, causing transverse oscillations of the electrons (see Fig. 1). As the rotational energy increases, due to the dependence of the gyrofrequency on the electron energy, condition (1) is violated, and cyclotron absorption saturates.

If we assume that the electromagnetic wave has the form of a quasi-harmonic wave with a slowly varying (compared to $\exp(i\omega_r t - ik_z z)$) amplitude $A(z,t)$, the electron-wave interaction in the model under consideration can be described by a system of averaged equations, well known from the literature [5–7]:

$$\frac{\partial a}{\partial \tau} - \frac{\partial a}{\partial Z} = -p, \tag{2}$$

$$\frac{\partial p}{\partial Z} + i|p|^2 p = a, \tag{3}$$

where

$$a = \frac{\sqrt{1 + \beta_z/\beta_{ph}}}{2\sqrt{2}G^{3/4}\beta_z^{3/2}\gamma_0} \frac{eAJ_{m-1}(\nu_n r_b/r_0)}{m_e c\omega_r} \tag{4}$$

is the normalized complex amplitude of the wave field,

$$p = \frac{\sqrt{\mu}p_\perp \exp(-i\omega_r t + ik_z z)}{G^{1/4} m_e c \gamma_0 \beta_z} \tag{5}$$

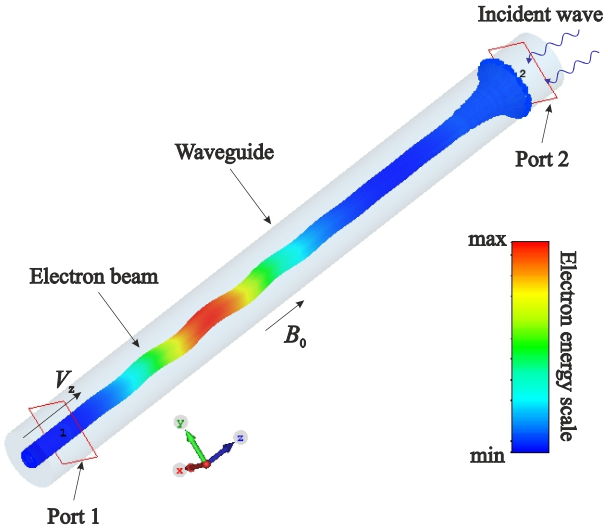

Fig. 1. Schematic of the cyclotron resonance interaction of an initially rectilinear electron beam with a counterpropagating electromagnetic wave. The pattern of electron trajectories was obtained by 3D PIC simulation (see section 4 for detail) (color online)

is the normalized complex transverse momentum of electrons $p_\perp = p_x + ip_y$,

$$Z = \frac{\sqrt{G}\omega_r z}{c} \tag{6}$$

and

$$\tau = \sqrt{G}\omega_r(t - z/V_z)\frac{\beta_g\beta_z}{\beta_z + \beta_g} \tag{7}$$

are dimensionless independent variables. Note that the introduction of the variable τ in accordance with (7) corresponds to a transition to the reference frame moving with the beam velocity.

In expressions (4)–(7)

$$\mu = \frac{\beta_z(1 - \beta_{ph}^{-2})}{2(1 + \beta_z/\beta_{ph})} \tag{8}$$

is the non-isochronism parameter; $\beta_z = V_z/c$, $\beta_{ph} = V_{ph}/c$ and $\beta_g = V_g/c$ are the unperturbed axial velocity of electrons, phase and group velocities of the wave, normalized to the speed of light c, respectively;

$$G = \frac{eI_b}{m_e c^3}\frac{2\mu(1 + \beta_z/\beta_{ph})^2}{\gamma_0\beta_{ph}^{-1}\beta_z^3}\frac{J_{m-1}^2(\nu_n r_b/r_0)}{J_m^2(\nu_n)(\nu_n^2 - m^2)} \tag{9}$$

is the parameter characterizing the coupling of electrons with the waveguide mode TE_{mn}; $\gamma_0 = (1 - \beta_z^2)^{-1/2}$ is the Lorentz factor of unperturbed electrons; I_b is the electron beam current; $J_m(x)$ is the Bessel function of order m, ν_n is the n-th root of the equation $dJ_m(x)/dx = 0$, r_b and r_0 are the beam injection radius and the waveguide radius, respectively.

Equation (2) describes the excitation of a wave by an electron beam, and equation (3) is the equation of electron motion averaged over the period of cyclotron oscillations $T_H = 2\pi/\omega_H^0$, where $\omega_H^0 = eB_0/(m_e\gamma_0)$ is the unperturbed cyclotron frequency. A detailed derivation of the main equations is presented in [5].

Since we are an initially rectilinear electron beam considering a rectilinear electron beam, the electrons have no rotational velocity at the entrance to the interaction space, i.e.,

$$p(Z = 0) = 0. \tag{10}$$

This allows us to describe the motion of all electrons using a single equation (3). As is well known, the equations for the resonant cyclotron interaction of electrons with a traveling wave allow for an integral of motion

$$|p_\perp||A|\sin\theta = \text{const}, \tag{11}$$

where $\theta = \omega_r t - k_z z + \vartheta + \alpha$, $\vartheta = arg(p_\perp)$ and $\alpha = arg(A)$ (see, for example, [18]). From (10) it follows that $|p_\perp||A|\sin\theta = 0$. During the interaction, electrons acquire a nonzero transverse momentum. Therefore, for condition (11) to be satisfied, it is necessary that $\sin\theta = 0$ for all electrons. This means that the transverse momenta of all electrons change equally during the interaction. For comparison: in cyclotron resonance masers (gyrotrons, gyro-TWTs, etc.), the wave interacts with initially rotating electrons, i.e., $p_\perp(z = 0) = p_0 e^{i\vartheta_0}$, where the rotation phases $\vartheta_0 = \vartheta(z = 0)$ are uniformly distributed from 0 to 2π. Thus, electrons with different ϑ_0 move differently, and it is necessary to solve separate equations of motion (3) for each electron.

At the right boundary of the system, at $Z = L$, an external continuous harmonic signal is applied, i.e.

$$a(Z = L) = a_0 \exp(i\delta\tau), \tag{12}$$

where a_0 is the normalized signal amplitude, and

$$\delta = \frac{1 + \beta_z/\beta_{ph} - \omega_H^0/\omega_r}{\beta_z\sqrt{G}} \tag{13}$$

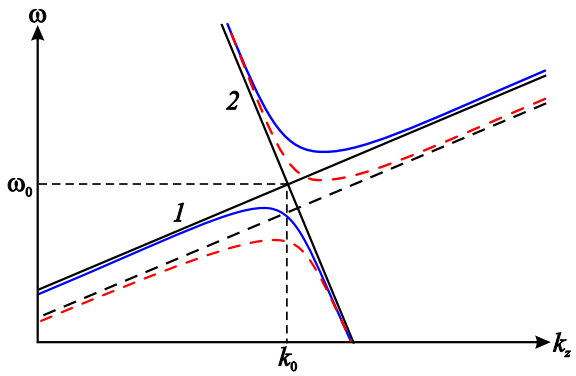

Fig. 2. Qualitative picture of the dispersion diagram. Asymptotes are the dispersion characteristic of the fast cyclotron wave $\omega = \omega_H + k_z V_z$ (line *1*) and the approximation of the dispersion characteristic of the waveguide mode $\omega = \omega_0 - (k + k_0)V_g$ (line *2*). Dashed lines illustrate the shift of the dispersion characteristic down in frequency with increasing the wave amplitude (color online)

is the normalized detuning of the carrier frequency ω_r from the resonant frequency.

An analysis of the solutions of equations (2), (3) in the form of monochromatic waves shows that there is a stopband associated with the complete cyclotron absorption of the incident wave [12, 13]. The stopband arises due to the interaction of the waveguide mode with the fast cyclotron wave in the electron beam (see the cyclotron resonance condition (1)), which is qualitatively demonstrated in the dispersion diagram shown in Fig. 2.

Due to the dependence of the cyclotron frequency on the electron energy $\omega_H = \omega_H(\gamma)$, cyclotron absorption is saturated. This is equivalent to the fact that the boundaries of the stopband shift downward in frequency with increasing wave amplitude. If the input signal frequency lies within the stopband and the input power is sufficiently low, the incident wave is completely absorbed. As the signal power increases, the critical frequency decreases, and when it becomes equal to the signal frequency, undamped wave propagation becomes possible. However, as shown in [12, 13], MI occurs, this is the corresponding monochromatic solution is unstable. The development of a MI usually leads to the formation of envelope solitons. Let us consider this process in more detail.

2. Nonlinear Schrödinger Equation

The most well-known example of envelope solitons is the soliton solutions of the nonlinear Schrödinger equation (NSE) [4,15,16]. The NSE is a reference equation describing the propagation of a quasi-harmonic wave in a cubic nonlinear medium. Using the NSE, one can approximately describe the dynamics of the system under consideration near critical frequencies, where the dispersion characteristic is approximated by a parabola (see Fig. 2).

We derive the NSE for the model under consideration using the well-known multiscale method [4]. Solutions to (2) and (3) are sought in the form of power series

$$\begin{aligned} a &= \varepsilon a_1 + \varepsilon^2 a_2 + \varepsilon^3 a_3 + ..., \\ p &= \varepsilon p_1 + \varepsilon^2 p_2 + \varepsilon^3 p_3 + ..., \end{aligned} \tag{14}$$

where ε is a small parameter. The expansion coefficients a_j, p_j, $j = 1, 2, ...$, are functions of the variables $Z_n = \varepsilon^n z$ and $T_n = \varepsilon^n t$, $n = 0, 1, 2, ...$, corresponding to different spatial and temporal scales.

After substituting (14) into equations (2) and (3), we extract terms of the same order of smallness in ε. Terms of order ε yield a linearized system of equations

$$\begin{aligned} \frac{\partial a_1}{\partial T_0} - \frac{\partial a_1}{\partial Z_0} &= -p_1, \\ \frac{\partial p_1}{\partial Z_0} &= a_1, \end{aligned} \tag{15}$$

which can be transformed into the form

$$\begin{aligned} \hat{L}a_1 &= 0, \\ p_1 &= \frac{\partial a_1}{\partial Z_0} - \frac{\partial a_1}{\partial T_0}. \end{aligned} \tag{16}$$

A linear operator is introduced here

$$\hat{L} = \frac{\partial}{\partial Z_0}\left(\frac{\partial}{\partial Z_0} - \frac{\partial}{\partial T_0}\right) - 1. \tag{17}$$

The solution of equations (16) should be chosen in the form of quasi-harmonic waves, the amplitude of which depends on the slow variables:

$$\begin{aligned} a_1 &= Ae^{i\theta} + \text{c.c.}, \\ p_1 &= -i(\omega + k)Ae^{i\theta} + \text{c.c.}, \end{aligned} \tag{18}$$

where $A{=}A(Z_1, Z_2, ..., T_1, T_2, ...)$ is the slowly varying complex amplitude, c.c. is the complex conjugate expression, $\theta = \omega T_0 - kZ_0$ is the carrier wave phase, and k and ω are related by the linear dispersion relation

$$(\omega + k)k = -1. \tag{19}$$

Recall that all variables are dimensionless, and by introducing the variable τ (7), we have effectively switched to a reference frame moving with the electrons.

Terms of order ε^2, after a series of transformations, lead to equations

$$\hat{L}a_2 = -\frac{\partial p_1}{\partial Z_1} - \frac{\partial^2 a_1}{\partial Z_0 \partial Z_1} + \frac{\partial^2 a_1}{\partial Z_0 \partial T_1}, \tag{20}$$

$$p_2 = \frac{\partial a_1}{\partial Z_0} - \frac{\partial a_1}{\partial T_0} + \frac{\partial a_2}{\partial Z_0} - \frac{\partial a_2}{\partial T_0}. \tag{21}$$

Substituting expressions (18) into (20) and requiring the elimination of secular terms proportional to $\exp(i\theta)$ on the right-hand side, we obtain an equation for the variable A:

$$\frac{\partial A}{\partial T_1} + v_g \frac{\partial A}{\partial Z_1} = 0, \tag{22}$$

where $v_g = -1 + 1/k^2$ is the group velocity. In this case, equation (20) takes the form $\hat{L}a_2 = 0$, which allows us to set $a_2 = 0$. Also from equation (22) we obtain

$$p_2 = \left(\frac{\partial A}{\partial Z_1} - \frac{\partial A}{\partial T_1}\right)e^{i\theta}. \tag{23}$$

In a similar treatment of terms of order ε^3, the requirement to eliminate secular terms leads to the NSE:

$$i\left(\frac{\partial A}{\partial T_2} + v_g \frac{\partial A}{\partial Z_2}\right) = \frac{\chi}{2}\frac{\partial^2 A}{\partial Z_1^2} + \beta|A|^2 A, \tag{24}$$

where $\chi = -2k^{-3}$ and $\beta = k^{-4}$ are the linear parameters of the group velocity dispersion and nonlinearity. In a frame of reference moving with group velocity v_g, (24) is simplified:

$$i\frac{\partial A}{\partial T_2} = \frac{\chi}{2}\frac{\partial^2 A}{\partial Z_1^2} + \beta|A|^2 A. \tag{25}$$

Equation (25) has a solution in the form of a wave with constant amplitude and a nonlinear frequency shift:

$$A = A_0 \exp\left(-i\beta |A_0|^2 T_2\right). \tag{26}$$

As is known (see, e.g., [4,15]), when the condition

$$\chi\beta > 0 \tag{27}$$

is satisfied the solution (26) is unstable, i.e., MI takes place. The nonlinearity parameter β is obviously always positive. This means that as the wave amplitude increases, the dispersion characteristic shifts toward lower frequencies. The group velocity dispersion parameter $\chi = \partial^2\omega/\partial k^2$ is positive on the upper branch of the dispersion characteristic and negative on the lower one (see Fig. 2). Thus, the upper branch exhibits MI, which is consistent with the conclusions obtained in the works [12, 13] by analyzing the nonlinear dispersion relation. At the same time, the lower branch corresponds to stable wave propagation.

As noted above, the nature of the instability (absolute or convective) plays a fundamental role. For the NSE (24), the nature of the instability was analyzed in the works [19, 20], where a criterion for absolute instability was obtained:

$$|A_0|^2 > \frac{v_g^2}{8\chi\beta}. \tag{28}$$

Substituting the expressions for v_g, β, and χ here, we obtain

$$|A_0|^2 > -\frac{k^7}{16}(-1 + k^{-2})^2. \tag{29}$$

Together with the dispersion relation (19), inequality (29) parametrically defines the boundary of the change in the nature of the MI on the parameter plane (ω, A_0), shown in Fig. 3. In [13], a similar problem was solved based on an analysis of the asymptotic form of unstable perturbations using the saddle-point method. This approach is more rigorous, but the position of the saddle points in the complex plane must be calculated numerically. In this case, we obtain a simple analytical relation. The results obtained using these approaches are quite close to each other, and in the region of small amplitudes, they practically coincide.

Thus, on the parameter plane (ω, A_0), we have the following picture (see Fig. 3). In region 1, cyclotron absorption of the wave occurs. The stopband boundaries are constructed according to the formulas obtained in [12]. Note that the upper boundary of the stopband corresponds to the dependence

$$|A_0|^2 = 2(2 - \omega), \tag{30}$$

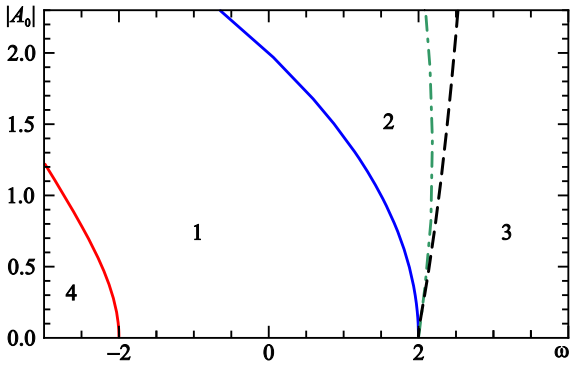

Fig. 3. Domains of different regimes of the wave propagation on the frequency – amplitude parameter plane: 1 — non-transmission, 2 — absolute MI, 3 — convective MI, 4 — no MI. The dashed line is the boundary of changing character of MI according to the condition (29). The dashed dotted line represents the boundary obtained by the analysis of the asymptotic form of unstable perturbations [13] (color online)

which exactly coincides with the frequency dependence of the amplitude of an immobile soliton (for more details, see section 3). In region 2, absolute MI occurs, and the signal is broken down into a train of envelope solitons. However, as the frequency increases, the MI changes from absolute to convective. In this case, after the transient process ends, stationary single-frequency signal propagation is established (region 3).

3. Soliton solutions

In the papers [5–8], soliton solutions to equations (2), (3) were found for the case of exact cyclotron resonance, that is, for $\delta = 0$. Since we will further investigate the dynamic regimes observed when the input signal frequency changes, it is necessary to consider more general solutions with a non-zero detuning from the resonance frequency. Thus, we will seek a solution in the form

$$\begin{aligned} a(Z,\tau) &= a(\zeta)e^{i\delta\tau}, \\ p(Z,\tau) &= p(\zeta)e^{i\delta\tau}, \end{aligned} \tag{31}$$

where $\zeta = Z - U\tau$, U is the wave propagation velocity. Substituting (31) into the original system of partial differential equations (2), (3) reduces it to a system of ordinary differential equations:

$$\begin{aligned} s\frac{da}{d\zeta} - i\delta a &= p, \\ \frac{dp}{d\zeta} + i|p|^2 p &= a, \end{aligned} \tag{32}$$

where $s = \sqrt{U+1}$. Equations (32) can be represented in Hamiltonian form

$$\begin{aligned} \frac{da}{d\zeta} &= i\frac{\partial H}{\partial a^*}, \\ \frac{dp}{d\zeta} &= -i\frac{\partial H}{\partial p^*}, \end{aligned} \tag{33}$$

where

$$H = \delta_s|a|^2 + \frac{|p|^4}{2} + i(ap^* - a^*p) \tag{34}$$

is the Hamiltonian, $\delta_s = \delta/s$. In addition to the Hamiltonian, which is always an integral of motion, the system (33) has another obvious integral

$$s^2|a|^2 - |p|^2 = \text{const}, \tag{35}$$

which reflects the fact that energy is transferred between the EMW and the transverse oscillations of the electrons in the system.

Suppose that $p(\zeta_0) = 0$ and $|a(\zeta_0)|^2 = I_0$ at some point in space $\zeta = \zeta_0$. Given this condition, it follows from (35) that

$$|p|^2 = s^2(I - I_0). \tag{36}$$

Here $I = |a|^2$. Also, in accordance with the boundary condition, we have $H = \delta_s I_0$. Then from (34) it follows that

$$\sin\psi = \frac{2\delta_s(I - I_0) + s^3(I - I_0)^2}{4\sqrt{I(I - I_0)}}, \tag{37}$$

where $\psi = \arg(a) - \arg(p)$. Taking into account relations (36) and (37), the system of equations (32) can be reduced to a single first-order ordinary differential equation:

$$\frac{dI}{d\zeta} = \pm\frac{1}{2s}\sqrt{I - I_0}\sqrt{16I - (I - I_0)(2\delta_s + s^3(I - I_0))^2}. \tag{38}$$

Solutions of equation (38) can be expressed in terms of Jacobi elliptic functions (for more details, see [12]). For $\delta > -2s$, setting $I_0 \to 0$, we can obtain solutions in the form of a soliton [12]

$$I = \frac{8 - 2\delta_s^2}{s^3\delta_s + 2s^3 \cosh\left[s^{-1}(\zeta - \zeta_{\max})\sqrt{4 - \delta_s^2}\right]}, \tag{39}$$

where $\zeta_{\max}$ denotes the position of the soliton maximum. Note that for $\delta = 0$, the solutions (39) coincide with those obtained in [5–8]. Examples of solutions for different values of δ and s are shown in Fig. 4.

The soliton amplitude $I_{\max} = I(\zeta_{\max})$ is equal to

$$I_{\max} = (4 - 2\delta_s)/s^3. \tag{40}$$

We define the soliton width as $D = 2\zeta_{1/2}$, where at $\zeta = \zeta_{\max} \pm \zeta_{1/2}$ the intensity is half of the maximum value, that is, $I(\zeta_{\max} \pm \zeta_{1/2}) = I_{\max}/2 = (2 - \delta_s)/s^3$. Taking into account (39), we can obtain that

$$D = \frac{2s}{\sqrt{4 - \delta_s^2}} \operatorname{arccosh}\left(\frac{4 + \delta_s}{2}\right). \tag{41}$$

A solution (39) exists when the frequency detuning parameter satisfies the inequality $-2s < \delta < 2s$. For $\delta \to 2s$, $I_{\max}$ tends to zero, and the characteristic soliton width tends to infinity. For $\delta \to -2s$, $I_{\max}$ reaches its maximum value $I_{\max} \to 8/s^3$, and the width, accordingly, reaches its minimum, $D = s$.

The case $s = 1$ corresponds to an immobile soliton. An immobile soliton solution exists for $-2 < \delta < 2$, that is, when the input signal frequency lies in the linear stopband (see Fig. 3). According to (40), the amplitude of an immobile soliton is

$$I_{\max} = 2(2 - \delta). \tag{42}$$

As shown in section 2, this expression defines the upper boundary of the stopband in the frequency-amplitude plane of the input signal (see (30)).

We also note that a soliton solution (39) exists under the condition $s > 0$, that is, for $U > -1$. Thus, solitons can move in both the positive ($U > 0$) and negative ($-1 < U < 0$) directions. As follows from (40), for the same carrier frequency δ, solitons traveling in the opposite direction have a higher intensity than solitons propagating along the electron beam, see Fig. 4, *b*.

The condition $U > -1$ means that the soliton velocity must not (in absolute value) exceed the phase velocity of linear waves (for more details, see [12,13]). Indeed, it is well known [21] that the soliton propagation velocity cannot coincide with the phase velocity $v_{ph}(\omega)$. If $v_{ph}(\omega) = U$ at some frequency, then the soliton is unstable: it decays, emitting waves at the frequency ω, which can be interpreted as an analog of Cherenkov radiation.

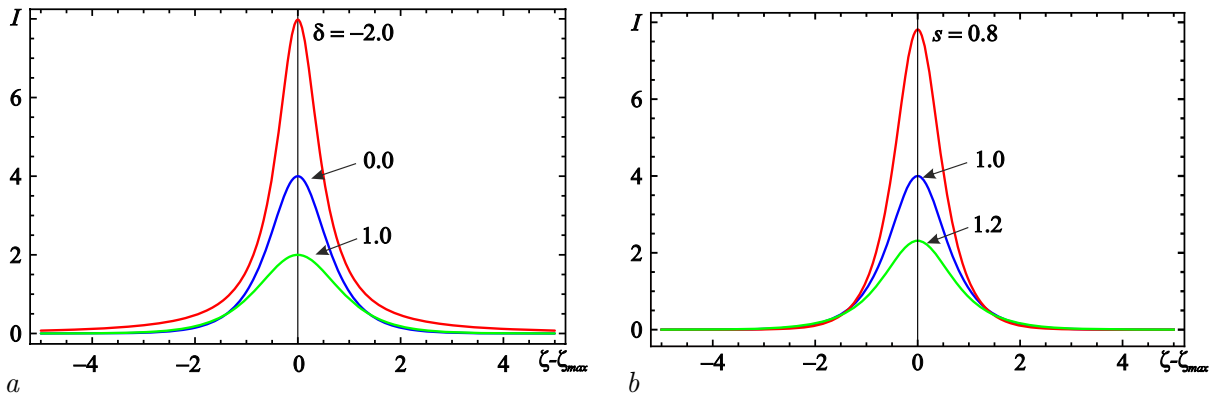

Fig. 4. Bright solitons (39) at different values of δ and $s = 1$ (*a*) and at different values of s and $\delta = 0$ (*b*) (color online)

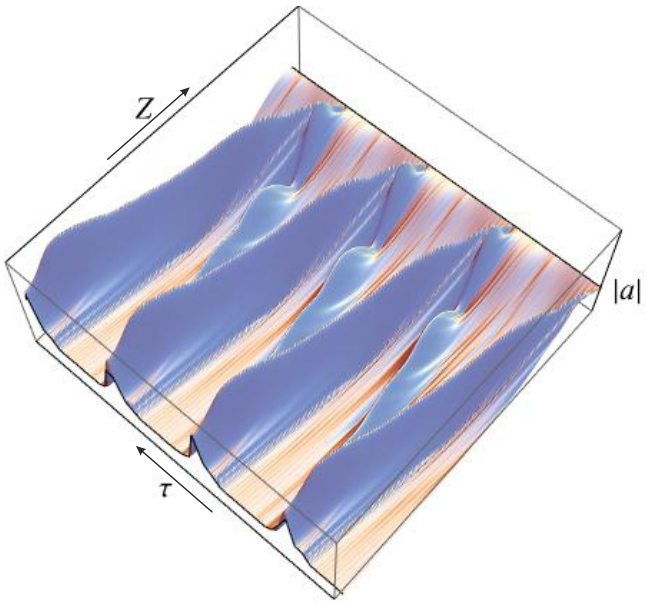

Fig. 5. Example of the spatio-temporal pattern of the normalized field amplitude in the regime of soliton train generation ($a_0 = 1$ and $\delta_0 = 1.48$), calculated by numerical integration of the averaged equations (color online)

As numerical simulations show, when the input signal frequency reaches the upper boundary of the stopband, the development of absolute-type MI causes the continuous input signal to disintegrate into a nearly periodic train of traveling solitons. An example of this process is illustrated in Fig. 5. It can be seen that the solitons form near the right end of the system and propagate in the opposite direction, that is, toward the electrons. Upon reaching the left end of the system, they are partially reflected and begin to move in the positive direction. The intensity of solitons moving toward the beam is significantly greater than that of reflected solitons, which is consistent with the analytical solution (39).

4. Three-dimensional PIC Simulation of Microwave SIT Soliton Formation

The most rigorous approach to studying electron-wave interaction is direct 3D Particle-in-Cell (PIC) simulation. This section presents the results of 3D PIC simulations using the CST Studio Suite software package [17]. This software package allows for the direct numerical integration of Maxwell's equations in conjunction with the relativistic equations of particle motion, taking into account the actual geometry of the interaction space.

A schematic of the system simulated using CST Studio Suite is shown in Fig. 1. A continuous harmonic signal of constant amplitude is applied from the right end of the system (port 2). Near the right boundary of the interaction space, the magnetic field gradually decreases to zero, and electrons are deposited on the inner walls of the waveguide, which acts as a collector. The output signal is taken at the left end of the system (port 1). Fig. 1 shows an image of electron trajectories in the interaction space, obtained in a 3D PIC simulation at a fixed point in time.

The simulation was performed for a cylindrical waveguide with a radius of $r_0 = 0.4$ mm and an interaction space length of $l = 26$ mm at a longitudinal magnetic field of $B_0 = 8.9$ T. A rectilinear electron beam with an injection radius of $r_b = 0.1$ mm, an initial energy of $E = 1.828$ keV, and a current of $I_b = 0.1$ A propagates along the system. A signal of constant power $P_0 = 140$ W with a frequency varying in the range of 240...242 GHz is fed into the system from the collector end.

The electron beam interacts with the circularly polarized TE_{11} mode of the cylindrical waveguide. The cyclotron frequency is $f_H = \omega_H/2\pi = 248.5$ GHz, the cutoff frequency of the waveguide TE_{11}-mode $f_c = c/(3.41r_0) = 219.8$ GHz. The axial velocity of electrons at the entrance to the interaction space is $V_z = \sqrt{2E/m_e} = 2.5 \cdot 10^7$ m/s (Lorentz factor is $\gamma = 1.0036$). Fig. 6 shows the dispersion characteristic

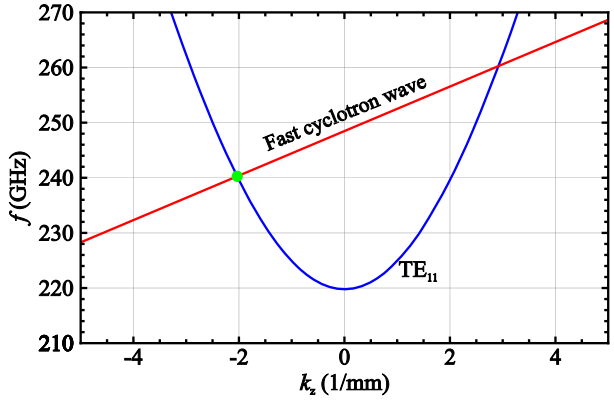

Fig. 6. Dispersion diagram of the fast cyclotron wave of the electron beam and the TE_{11} waveguide mode at parameters used in 3D PIC simulations. Point of the exact cyclotron resonance is shown by circle (color online)

of the TE_{11} mode

$$f^2 = f_c^2 + \frac{ck_z}{2\pi}^2 \tag{43}$$

and the dispersion characteristic of the fast cyclotron wave

$$f = f_H + V_z \frac{k_z}{2\pi}. \tag{44}$$

The cyclotron resonance condition corresponds to the intersection of the beam line (44) and the dispersion curve (43). With the chosen parameters, the resonant frequency is $f_0 = 240.3$ GHz.

To achieve circular polarization of the incident wave, two orthogonal linearly polarized TE_{11} modes with identical amplitudes and a phase difference of 90° were excited at port 2. The average input signal power was fixed at P_0=140 W. Modern sub-THz gyrotrons are capable of delivering a power of this order in continuous-wave regime [22].

In numerical experiments, the input signal frequency f was increased, starting from a value f_0 corresponding to the exact cyclotron resonance. Fig. 7 illustrates the characteristic oscillation regimes for different values of f. It shows the time dependences of the output signal at port 1 and the reflected signal at port 2. These signals, like the input signal, are the sum of two linearly polarized TE_{11} modes. For clarity, Fig. 7 shows oscillograms for the electric field component linearly polarized along the x axis.

At precise cyclotron resonance, when $f = f_0 = 240.3$ GHz, wave absorption is observed (see Fig. 7, *a*). In this case, the input signal, passing through the system, is almost completely attenuated, and the output signal power at port 1 after the transient process tends to zero. As the input signal frequency increases, wave absorption is replaced by non-stationary self-modulation. The generation of a nearly periodic pulse train is demonstrated in Fig. 7, *b*. According to the theoretical analysis, this wave propagation regime corresponds to absolute MI. The duration of the generated pulses is 3–4 ns. Note that the peak amplitude of the pulses exceeds the amplitude of the input signal (dashed lines in Fig. 7). The peak power of the output signal is approximately 200 W with an input power of 140 W.

Finally, at even higher frequencies, a transition from absolute instability to convective instability occurs. Figure 7, c shows that after several damped oscillations, steady-state wave propagation is established. The steady-state output power is approximately 75 % of the input signal power, since part of the signal is reflected (see the oscillogram of the reflected signal in Figure 7, c). The output signal spectrum in steady-state regime contains only the input signal frequency (Figure 8, a).

At the same time, during absolute instability, when self-modulation regime, i.e., multi-frequency oscillation regime, is established, the output signal spectrum is enriched with new independent spectral components, as shown in Figure 8, b. The modulation frequency, that is, the distance between adjacent peaks in the signal spectrum, is 0.19 GHz, which is approximately equal to $1/T$, where $T \approx 5.25$ ns is the pulse repetition period (see the output signal oscillogram in Fig. 7, *b*).

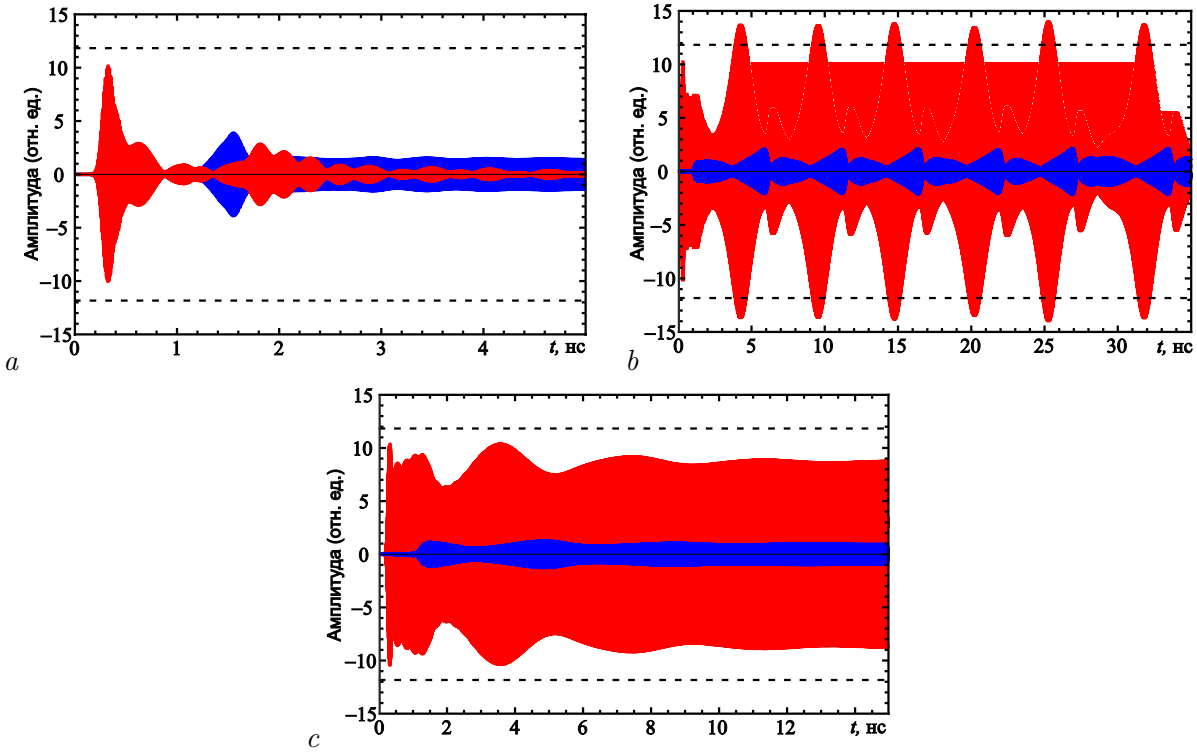

Fig. 7. Results of 3D PIC simulation. Waveforms of the output signal in port 1 (red curves) and the reflected signal in port 2 (blue curves) in different regimes of the wave propagation: a — $f = 240.3$ GHz (the exact cyclotron resonance), the regime of cyclotron absorption; b — $f = 241.3$ GHz, the regime of soliton train generation (absolute MI), c — $f = 241.65$ GHz, the regime of stationary signal transmission (convective MI). Horizontal dashed lines show the input signal level (color online)

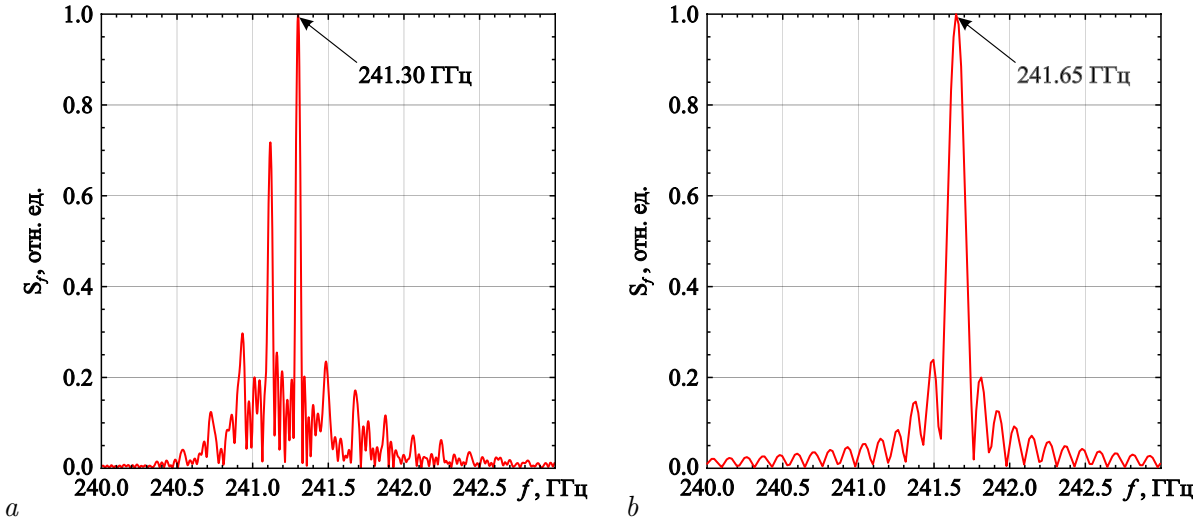

Fig. 8. Spectra of the output signal in port 2: a — the regime of stationary transmission of the wave ($f = 241.65$ GHz), b — the regime of soliton train generation ($f = 241.3$ GHz)

Conclusion

This paper develops a theory of MI for the interaction of EMW with a counterpropagating of unexcited electron oscillators under cyclotron resonance conditions. NSE is derived that describes the

dynamics of a slowly varying wave amplitude whose frequency lies near the stopband boundary. Analysis shows that MI occurs near the upper boundary, which can lead to the formation of envelope solitons. Also, by analogy with the results of [19,20], a simple analytical expression is derived for the transition boundary from absolute instability to convective instability. Studying the nature of MI allows us to determine the conditions for the transformation of a continuous signal of constant amplitude into a train of SIT solitons.

The results of direct 3D PIC simulation of electron-wave interaction are consistent with the conclusions obtained from the analysis of the averaged system of equations. In particular, as the input signal frequency increases, the same sequence of transitions between different dynamic regimes is observed. Above the stopband boundary, non-stationary self-modulation regimes occur, associated with the development of absolute-type MI, which can lead to the formation of soliton-like pulse trains. As the input signal transmission frequency increases, self-modulation gives way to a stationary, single-frequency signal, due to the change in the nature of the MI from absolute to convective. 3D PIC simulation demonstrates the possibility of converting a harmonic signal into a nearly periodic train of nanosecond pulses. This effect is of interest for generating frequency combs in the microwave range.

References

1. Ginzburg NS, Zotova IV, Sergeev AS, Kocharovskaya ER, Yalandin MI, Shunailov SA, Sharypov KA, Ryskin NM. The amplification, compression, and self-induced transparency effects for the ultrashort electromagnetic pulses propagating along quasi-stationary electron beams. Radiophys. Quantum Electron. 2012;54(8–9):532–547. DOI: 0033-8443/12/5408-0532.
2. Ginzburg NS, Zotova IV, Cross AW, Phelps ADR, Yalandin MI, Rostov VV. Generation, amplification, and nonlinear self-compression of powerful superradiance pulses. IEEE Trans. Plasma Sci. 2013;41(4):646–660. DOI: 10.1109/TPS.2013.2252369.
3. McCall SL, Hahn EL. Self-induced transparency by pulsed coherent light. Phys. Rev. Lett. 1967;18(21):908–911. DOI: 10.1103/PhysRevLett.18.908.
4. Ryskin NM, Trubetskov DI. Nonlinear Waves. M.: URSS; 2021. 312 p. (in Russian).
5. Ginzburg NS, Zotova IV, Sergeev AS. Self-induced transparency, compression, and stopping of electromagnetic pulses interacting with beams of unexcited classical oscillators. J.Exp. Theor. Phys. 2011;113(5):772–780. DOI: 10.1134/S1063776111140147.
6. Zotova IV, Ginzburg NS, Zheleznov IV, Sergeev AS. Modulation of high-intensity microwave radiation during its resonant interaction with counterflow of nonexcited cyclotron oscillators. Tech. Phys. Lett. 2014;40:495–498. DOI: 10.1134/S1063785014060285.
7. Zotova IV, Ginzburg NS, Sergeev AS, Kocharovskaya ER, Zaslavsky VYu. Conversion of an electromagnetic wave into a periodic train of solitons under cyclotron resonance interaction with a backward beam of unexcited electron-oscillators. Phys. Rev. Lett. 2014;113:143901. DOI: 10.1103/PhysRevLett.113.143901.
8. Ginzburg NS, Zotova IV, Kocharovskaya ER, Sergeev AS, Zheleznov IV, Zaslavsky VYu. Self-induced transparency solitons and dissipative solitons in microwave electronic systems. Radiophys. Quantum Electron. 2021;63:716–741. DOI: 10.1007/s11141-021-10092-w.
9. Gaponov AV, Petelin MI, Yulpatov VK. The induced radiation of excited classical oscillators and its use in high-frequency electronics. Radiophys. Quantum Electron. 1967;10(9–10): 1414–1453. DOI: 10.1007/BF01031607.
10. Benirschke DJ, Han N, Burghoff D. Frequency comb ptychoscopy. Nat. Commun. 2021;12: 4244. DOI: 10.1038/s41467-021-24471-4.
11. Hagmann MJ. Scanning frequency comb microscopy — A new method in scanning probe microscopy. AIP Advances. 2018;8(12):125203. DOI: 10.1063/1.5047440.
12. Rostuntsova AA, Ryskin NM, Zotova IV, Ginzburg NS. Modulation instability of an electromagnetic wave interacting with a counterpropagating electron beam under condition of cyclotron resonance absorption. Phys. Rev. E. 2022;106:014214. DOI: 10.1103/PhysRevE.106.014214.
13. Rostuntsova AA, Ryskin NM. Study of character of modulation instability in cyclotron resonance interaction of an electromagnetic wave with a counterpropagating rectilinear electron beam. Izvestiya VUZ. Applied Nonlinear Dynamics. 2023;31(5):597–609. DOI: 10.18500/0869-6632-003067.
14. Benjamin TB. Instability of periodic wavetrains in nonlinear dispersive systems. Proc. Roy. Soc. A. 1967;299:59–75. DOI: 10.1098/rspa.1967.0123.

15. Ostrovsky LA, Potapov AI. Modulated Waves: Theory and Applications. Baltimore: The Johns Hopkins University Press; 1999. 369 p.
16. Zakharov VE, Ostrovsky LA. Modulation instability: The beginning. Physica D. 2009;238(5): 540–548. DOI: 10.1016/j.physd.2008.12.002.
17. CST Studio Suite Electromagnetic Field Simulation Software, Dassault Systèmes, Vélizy Villacoublay, France, 2020. [Electronic resource]. Available from: https://www.3ds.com/ products/simulia/cst-studio-suite
18. Nusinovich GS, Korol M, Jerby E. Theory of the anomalous Doppler cyclotron-resonance maser amplifier with tapered parameters. Phys. Rev. E. 1999;59(2):2311–2321. DOI: 10.1103/ PhysRevE.59.2311.
19. Balyakin AA, Ryskin NM. A change in the character of modulation instability in the vicinity of a critical frequency. Tech. Phys. Lett. 2004;30:175–177. DOI: 10.1134/1.1707158.
20. Balyakin AA, Ryskin NM. Modulation instability in a nonlinear dispersive medium near cut-off frequency. Nonlinear Phenomena in Complex Systems. 2004;7(1):34–42.
21. Zakharov VE, Kuznetsov EA. Optical solitons and quasisolitons. JETP. 1998;86(5):1035–1046. DOI: 10.1134/1.558551.
22. Glyavin MYu, Denisov GG, Zapevalov VE, Kuftin AN, Luchinin AG, Manuilov VN, Morozkin MV, Sedov AS, Chirkov AV. Terahertz gyrotrons: state of the art and prospects. Journal of Communications Technology and Electronics. 2014;59(8):792–797. DOI: 10.1134/S1064 226914080075.